Inorganic Chemistry

Article

pubs.acs.org/IC

Thermodynamics of the Cu^{II} μ-Thiolate and Cu^{I} Disulfide Equilibrium: A Combined Experimental and Theoretical Study

Erica C.M. Ording-Wenker,[†] Martijn van der Plas,[†] Maxime A. Siegler,[‡] Sylvestre Bonnet,[†] F. Matthias Bickelhaupt,[§,∥] Célia Fonseca Guerra,*[,§] and Elisabeth Bouwman*[,†]

[†]Leiden Institute of Chemistry, Gorlaeus Laboratories, Leiden University, P.O. Box 9502, 2300 RA Leiden, The Netherlands

[‡]Department of Chemistry, Johns Hopkins University, 3400 N. Charles Street, Baltimore, Maryland 21218, United States

[§]Department of Theoretical Chemistry, Amsterdam Center for Multiscale Modeling (ACMM), VU University Amsterdam, De Boelelaan 1083, 1081 HV Amsterdam, The Netherlands

[∥]Institute for Molecules and Materials, Radboud University Nijmegen, Heyendaalseweg 135, 6525 AJ Nijmegen, The Netherlands

Supporting Information

ABSTRACT: The redox equilibrium between dinuclear Cu^{II} μ-thiolate and Cu^{I} disulfide structures has been analyzed experimentally and via DFT calculations. Two new ligands, $\mathbf{L^2SSL^2}$ and $\mathbf{L^4SSL^4}$, and their Cu^{II} μ-thiolate and Cu^{I} disulfide complexes were synthesized. For $\mathbf{L^2SSL^2}$, these two redox-isomeric copper species are shown to be in equilibrium, which depends on both temperature and solvent. For $\mathbf{L^4SSL^4}$ the μ-thiolate species forms as the kinetic product and further evolves into the disulfide complex under thermodynamic control, which creates the unprecedented possibility to compare both species under the same reaction conditions. The energies of the μ-thiolate and disulfide complexes for two series of related ligands have been calculated with DFT; the results rationalize the experimentally observed structures, and emphasize the important role that steric requirements play in the formation of the Cu^{II} thiolate structure.

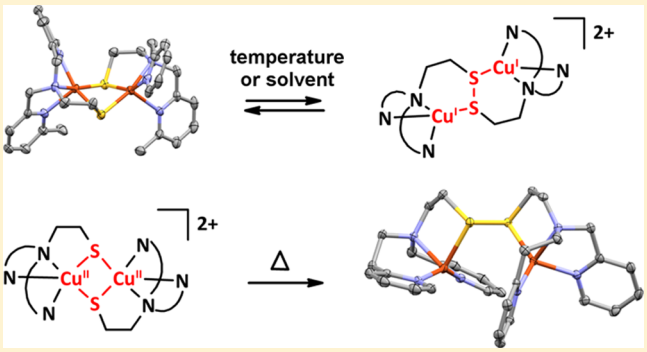

1. INTRODUCTION

Redox reactions are frequently occurring in biological systems and are the basis for important electron-transfer reactions as for example the binding and reduction of molecules such as dioxygen, nitrite, and nitrous oxide.[1] Many of these reactions involve sulfur-containing compounds, such as cysteine or glutathione, which are participating in a thiolate−disulfide equilibrium.[2−5] This thiolate−disulfide equilibrium can be tuned by the presence of a metal center. For example, copper is involved in sulfur-based redox reactions in the biological Cu_A site of cytochrome c oxidase (CcO)[6−8] and nitrous oxide reductase.[9] The active sites contain two copper centers that are bridged by thiolate sulfurs of cysteine residues that facilitate the redox cycling between $Cu^{1.5}Cu^{1.5}$ and $Cu^{I}Cu^{I}$ with minor geometrical changes.[10] The copper delivery to the Cu_A site of CcO is carried out by Sco proteins using a mechanism which is suggested to use a copper thiolate/disulfide conversion.[11−13] These thiolate/disulfide conversions with copper are also involved in controlling the concentrations of reactive oxygen species (ROS) associated with aging, cancer, and neurological disorders such as Alzheimer's disease.[14−18] As a result of oxidative stress, oxidation products of cysteine comprise sulfonic acid, sulfates, sulfones, and sulfoxides.[2] Previous research by our group has shown that dinuclear Cu^{II} μ-thiolate species, resembling the Cu_A site, react with oxygen to form Cu^{II} sulfinate and Cu^{II} sulfonate complexes.[19] Controlling the interconversion between the Cu^{II} μ-thiolate and Cu^{I} disulfide form of dinuclear copper complexes would allow for understanding copper−sulfur redox reactions occurring in natural systems. Coordination chemists have tried gaining information about the thiolate/disulfide redox reactions by synthesizing biomimetic (dinuclear) Cu^{II} thiolate complexes.[20−22] However, these complexes are difficult to isolate and characterize, since they are often not stable and react further to form dinuclear Cu^{I} disulfide compounds.[23] A few reports describe how to shift the Cu^{II} thiolate−Cu^{I} disulfide equilibrium by adding chloride ions[24,25] or protons,[16] or by changing the solvent.[26] In addition, minute changes in the ligand structure were shown to induce the preferential formation of either a dinuclear Cu^{II} μ-thiolate compound (Figure 1, conformation **A**), a Cu^{I} *transoid*-disulfide (Figure 1, conformation **B**), or a Cu^{I} *cisoid*-disulfide complex (Figure 1, conformation **C**).[27] Up to now, there is limited understanding about why or when the Cu^{II} thiolate complex forms, i.e., whether the electrons are located on copper or sulfur, and as far as we know there are no theoretical

Received: May 8, 2014
Published: August 4, 2014

   dx.doi.org/10.1021/ic501060w | *Inorg. Chem.* 2014, 53, 8494−8504

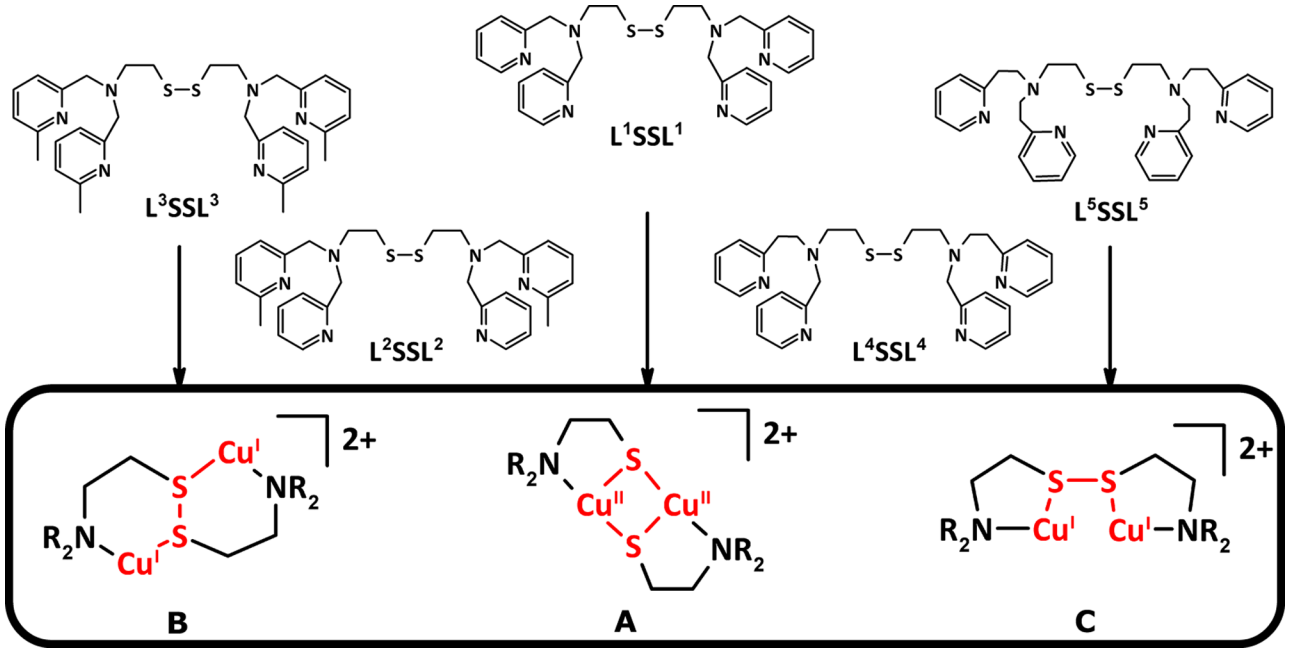

Figure 1. Schematic overview of the ligands discussed in this paper and the complexes that are formed when L^1SSL^1, L^3SSL^3, and L^5SSL^5 are reacted with $[Cu(CH_3CN)_4]^+$.[27]

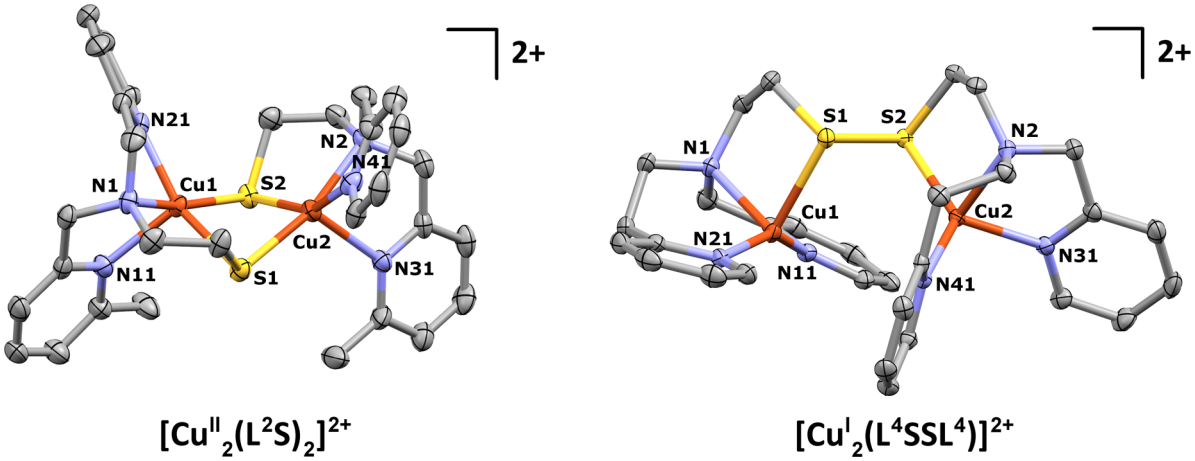

$[Cu^{II}_2(L^2S)_2]^{2+}$ $[Cu^{I}_2(L^4SSL^4)]^{2+}$

Figure 2. Displacement ellipsoid plots (50% probability level) of the cationic parts of $[Cu^{II}_2(L^2S)_2](BF_4)_2{\cdot}C_3H_6O$ and $[Cu^{I}_2(L^4SSL^4)](BF_4)_2$ at 110(2) K. Hydrogen atoms are omitted for clarity.

descriptions of these dinuclear structures. We considered dipyridylamine ligands as an ideal system to understand the redox equilibrium between the Cu^{II} μ-thiolate and Cu^{I} disulfide form of their dinuclear copper complexes, as small ligand variations have been shown to induce the formation of three different species. Thus, the two new asymmetric ligands L^2SSL^2 and L^4SSL^4 were designed and synthesized. These ligands combine structural elements of the reported ligand L^1SSL^1 with either L^3SSL^3 or L^5SSL^5 (Figure 1), resulting in two series of ligands with either an increasing number of C6-methylated pyridines or an increasing number of ethylene bridges between the amine nitrogen and the pyridine rings. We report the unprecedented effects of such small variations on the type of dinuclear copper complexes experimentally formed. DFT calculations have been carried out to quantify the different energies associated with the formation of these species.

2. RESULTS

2.1. Ligand Synthesis. The ligands L^2SSL^2 and L^4SSL^4 were synthesized via the precursor bis(2-(*N*-pyridylmethyl)-aminoethyl) disulfide ($L^{NH}SSL^{NH}$), which was synthesized following a literature procedure.[25] The synthetic scheme is provided in the Supporting Information, Scheme S1. L^2SSL^2 was formed by reductive amination of $L^{NH}SSL^{NH}$ with 2 equiv of 6-methyl-2-pyridinecarboxaldehyde. The crude product contained side products which were shown by ^{1}H NMR and MS spectra to have originated from scrambling of the 2-pyridyl and 6-methyl-2-pyridyl groups during the reaction. After purification by column chromatography, L^2SSL^2 was obtained as a cream-colored powder that was recrystallized from petroleum ether. L^4SSL^4 was synthesized by alkylation of $L^{NH}SSL^{NH}$ with 2-vinylpyridine. The pure product was obtained after column chromatography as a light-brown oil, which darkens over longer periods of time (weeks) indicating degradation of the product.

dx.doi.org/10.1021/ic501060w | Inorg. Chem. 2014, 53, 8494−8504

Table 1. Selected Bond Distances and Angles of $[Cu^{II}_2(L^2S)_2](BF_4)_2{\cdot}C_3H_6O$ and $[Cu^{I}_2(L^4SSL^4)](BF_4)_2$

bond distance (Å)			bond angle (deg)			dihedral angle (deg)		
	$[Cu^{II}(L^2S)_2]^{2+}$	$[Cu^{I}(L^4SSL^4)]^{2+}$		$[Cu^{II}(L^2S)_2]^{2+}$	$[Cu^{I}(L^4SSL^4)]^{2+}$		$[Cu^{II}(L^2S)_2]^{2+}$	$[Cu^{I}(L^4SSL^4)]^{2+}$
Cu1−Cu2	3.0444(12)	3.8988(3)	Cu1−S1−S2	46.43(5)	97.88(2)	Cu1−S1−S2−Cu2	132.99(9)	−77.015(19)
S1−S2	3.164(2)	2.0643(6)	Cu2−S2−S1	46.44(5)	96.18(2)	Cu1−S1−Cu2−S2	−32.26(7)	104.83
Cu1−S1	2.2920(18)	2.4155(5)	Cu1−S1−Cu2	83.16(6)	86.82(2)			
Cu1−S2	2.2952(18)	3.3858(5)	Cu1−S2−Cu2	83.21(6)	85.31(2)			
Cu1−N1	2.109(6)	2.1625(15)	S1−Cu1−S2	87.22(7)	37.15(1)			
Cu1−N11	2.256(6)	1.9669(15)	S1−Cu1−N1	88.65(16)	86.97(4)			
Cu1−N21	2.040(6)	1.9449(15)	S1−Cu2−S2	87.27(7)	39.93(2)			
Cu2−S1	2.2954(18)	3.1973(5)	S1−Cu1−N11	98.22(16)	109.56(4)			
Cu2−S2	2.2897(19)	2.2295(5)	S1−Cu1−N21	151.61(18)	101.55(5)			
Cu2−N2	2.104(6)	2.1421(14)	S2−Cu1−N1	166.74(18)	93.76(4)			
Cu2−N31	2.236(6)	2.0198(15)	S2−Cu1−N11	113.53(15)	73.97(5)			
Cu2−N41	2.027(6)	1.9950(14)	S2−Cu1−N21	99.05(18)	135.00(5)			
			N1−Cu1−N11	79.5(2)	84.31(6)			
			N1−Cu1−N21	78.9(2)	102.36(6)			
			N11−Cu1−N21	104.4(2)	148.52(6)			
			S1−Cu2−N2	164.93(17)	91.84(4)			
			S1−Cu2−N31	115.75(16)	161.81(5)			
			S1−Cu2−N41	97.80(18)	88.77(4)			
			S2−Cu2−N2	88.49(16)	91.03(4)			
			S2−Cu2−N31	100.87(16)	122.11(4)			
			S2−Cu2−N41	152.83(18)	127.83(4)			
			N2−Cu2−N31	79.3(2)	84.77(6)			
			N2−Cu2−N41	79.7(2)	101.66(6)			
			N31−Cu2−N41	100.8(2)	109.43(6)			

2.2. Synthesis and Structures of $[Cu^{II}_2(L^2S)_2](BF_4)_2{\cdot}C_3H_6O$ and $[Cu^{I}_2(L^4SSL^4)](BF_4)_2$. Addition of $[Cu(CH_3CN)_4]^+$ to a solution of L^2SSL^2 in weakly or non-coordinating solvents such as dichloromethane or acetone results in a color change from light yellow to dark green. Slow vapor diffusion of pentane into an acetone solution of the complex resulted in the formation of black crystals suitable for X-ray structure determination. The single crystal X-ray analysis confirms the structure of a dinuclear Cu^{II} μ-thiolate complex with the formula $[Cu^{II}_2(L^2S)_2](BF_4)_2{\cdot}C_3H_6O$, which is characterized by the relatively long S−S distance of 3.164(2) Å, whereas a disulfide bond in a Cu^{I} complex is on average ∼2.1 Å.[23,25,27] In contrast, when $[Cu(CH_3CN)_4]^+$ was added to L^4SSL^4 a bright green solution was obtained independent of the solvent used. When this solution was heated under anaerobic conditions, the color gradually evolved from green to brown. Crystals suitable for X-ray structure determination were obtained by vapor diffusion of hexane into a methanol solution. These crystals appeared to be a Cu^{I} disulfide structure of type **C** (see Figure 1) with the chemical formula $[Cu^{I}_2(L^4SSL^4)](BF_4)_2$. Displacement ellipsoid plots of the cationic dinuclear structures of $[Cu^{II}_2(L^2S)_2]^{2+}$ and $[Cu^{I}_2(L^4SSL^4)]^{2+}$ are depicted in Figure 2; crystallographic data can be found in the Supporting Information, Table S1, and selected bond distances and angles are given in Table 1.

The complex $[Cu^{II}_2(L^2S)_2](BF_4)_2{\cdot}C_3H_6O$ crystallizes in the orthorhombic space group $Pna2_1$ with two crystallographically independent dinuclear complexes and two acetone molecules in the asymmetric unit. Three of the four crystallographically independent BF_4^- counterions and one of the two acetone solvent molecules are disordered over two orientations. The occupancy factors of their major components refine to 0.843(9), 0.676(12), and 0.69(3) for BF_4^- and 0.58(4) for the acetone molecule. Only one of the two crystallographically independent cations is discussed, as both cations are very similar. The Cu^{II} ions are in N_3S_2 coordination environments with slightly distorted square-pyramidal geometries. The basal planes are formed by the two thiolate sulfur atoms, the amine nitrogen atom and the unsubstituted pyridyl nitrogen atom; the pyramids are edge-sharing through the bridging thiolate sulfurs. The nitrogen atom of the 6-methylpyridyl group is located at the axial position, and both 6-methyl-2-pyridyl groups are located on the same side of the Cu_2S_2 average plane. The copper−sulfur distances are all similar (∼2.29 Å). The Cu−Cu distance is 3.0444(12), which is slightly longer than reported for similar complexes such as $[Cu^{II}_2(L^1S)_2]^{2+}$ (2.960 Å).[25,27] The Cu−S−Cu−S central unit is in a butterfly arrangement with a dihedral angle of 32.26(7)°.

The complex $[Cu^{I}_2(L^4SSL^4)](BF_4)_2$ crystallizes in the triclinic space group $P\bar{1}$. The two copper centers are found in different distorted four-coordinate geometries. The Cu1 center is in a "saw-horse" or "double T-shaped" geometry. The di(pyridyl)amine group is coordinated in a meridional-type fashion, forming a T-shaped coordination at the copper ion in which the pyridyl groups are roughly in the same plane (N11−Cu1−N21 is 148.52(6)°). The disulfide sulfur atom, together with the pyridyl nitrogen atoms, forms the second T-shape, perpendicular to the other one. The Cu2 center is coordinated in a trigonal-pyramidal geometry, with the two pyridyl nitrogen atoms and the sulfur atom in the trigonal plane, and the amine nitrogen atom in the axial position. Interestingly, an additional copper−hydrogen interaction is present: the pyridyl hydrogen H16 (ortho to N11) is at a distance to Cu2 of ca. 2.98 Å; similar Cu−H interactions have been reported with distances ranging from 2.36 to 2.91 Å.[28−31] When this additional interaction is taken into account, the geometry of Cu2 can be considered as a trigonal bipyramid. The Cu1−Cu2 distance is 3.8988(3) Å, which is similar to what has been reported for

dx.doi.org/10.1021/ic501060w | Inorg. Chem. 2014, 53, 8494−8504

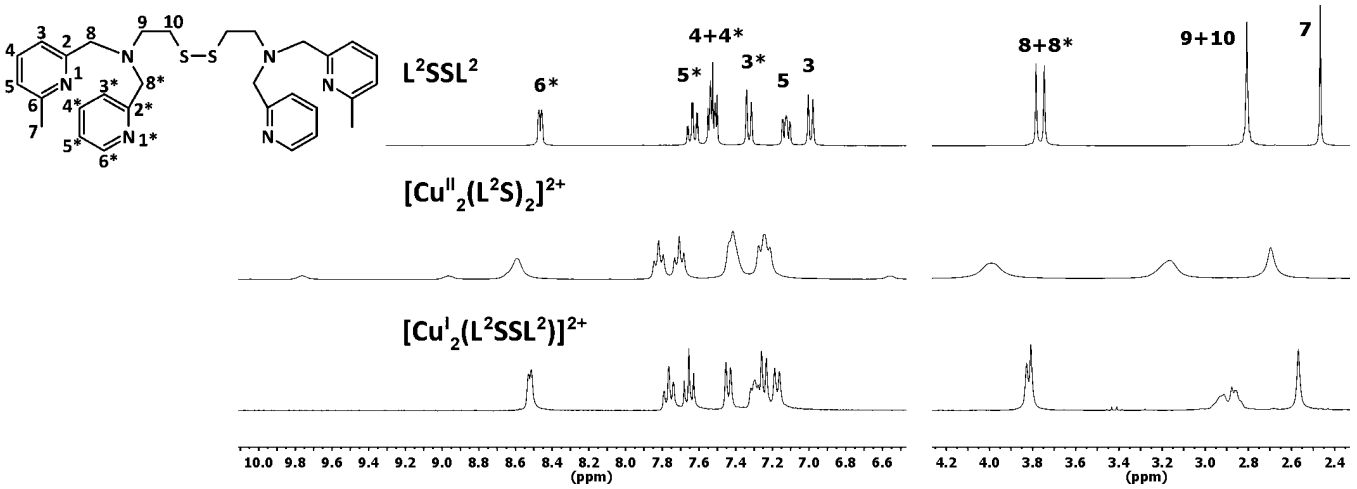

Figure 3. ^{1}H NMR spectra of $\mathbf{L^2SSL^2}$ and $[Cu^{II}_2(\mathbf{L^2S})_2]^{2+}$ in CD_2Cl_2 and $[Cu^{I}_2(\mathbf{L^2SSL^2})]^{2+}$ in CD_3CN at RT.

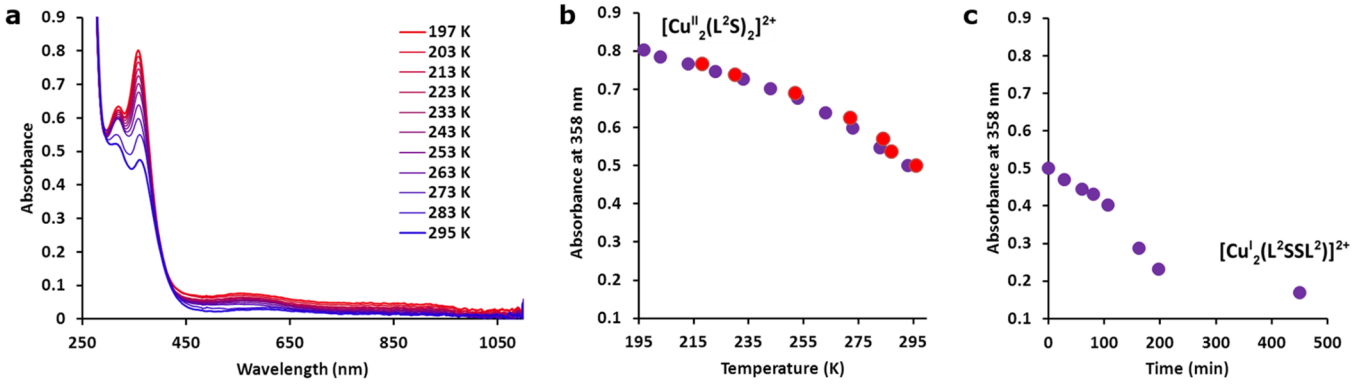

Figure 4. (a) UV–vis spectra of $[Cu(CH_3CN)_4]^+$ + $\mathbf{L^2SSL^2}$ at different temperatures between 197 and 295 K. The absorption of the $Cu^{II} \leftarrow S$ LMCT at 358 nm (b) plotted vs temperature while cooling down (purple) and heating (red) and (c) plotted vs time while heating at 333 K. Spectra were measured in methanol at 1 mM [Cu] recorded with a transmission dip probe path length of 2.0 mm.

$[Cu^{I}_2(\mathbf{L^5SSL^5})]^{2+}$.[27] The Cu–S distance is rather different for each copper center with a longer 2.4155(5) Å distance for Cu1–S1 compared to 2.2295(5) Å for Cu2–S2, the latter being more in agreement with the distances reported previously.[23,27] The different Cu–S distances must be ascribed to the asymmetric nature of the structure and the different geometries of the copper ions. The computed structures of $[Cu^{I}_2(\mathbf{L^4SSL^4})]^{2+}$ in conformation **C** (see section 2.4) show a similar difference in Cu–S distances of 2.17 and 2.25 Å in both the gas phase as well as in acetonitrile. The Cu–H interaction is not found in these calculated structures. Even though the difference in Cu–S distances is smaller in the calculated structures, the results indicate that sterics play a role in the asymmetry of this complex.

2.3. Solution Studies of $[Cu^{II}_2(\mathbf{L^2S})_2]^{2+}$ and $[Cu^{I}_2(\mathbf{L^4SSL^4})]^{2+}$. When a more polar (or more strongly coordinating) solvent such as acetonitrile is used in the reaction between $[Cu(CH_3CN)_4]^+$ and $\mathbf{L^2SSL^2}$, a pale greenish-yellow solution is obtained instead of the dark green solution obtained in acetone or dichloromethane. UV–vis spectra (Supporting Information, Figures S7 and S8) of the dark green μ-thiolate complex $[Cu^{II}_2(\mathbf{L^2S})_2]^{2+}$ in dichloromethane show absorption bands at 261 nm (ε = 17 200 M^{-1} cm^{-1}) attributed to the $\pi^* \leftarrow \pi$ transition of the pyridyl groups, two bands at 300 nm (ε = 7100 M^{-1} cm^{-1}) and 358 nm (ε = 4200 M^{-1} cm^{-1}) attributed to $Cu^{II} \leftarrow$ S LMCT transitions, and three bands at 500 nm (ε = 1200 M^{-1} cm^{-1}), 627 nm (ε = 1100 M^{-1} cm^{-1}), and 928 nm (ε = 410 M^{-1} cm^{-1}) attributed to copper d–d transitions. In acetonitrile, a $\pi^* \leftarrow \pi$ transition is observed at 257 nm (ε = 7950 M^{-1} cm^{-1}) as well as a $Cu^{I} \leftarrow$ S LMCT band at 309 nm (ε = 3150 M^{-1} cm^{-1}), but no d–d transitions are present at higher wavelengths. The lack of d–d transitions in acetonitrile indicates the presence of Cu^{I} instead of Cu^{II} ions. The ^{1}H NMR spectra of the copper complexes in different solvents were recorded (Figure 3) and compared to the spectrum of the free ligand.

NMR resonances are observed in the diamagnetic region for $[Cu^{II}_2(\mathbf{L^2S})_2]^{2+}$ in CD_2Cl_2, and the compound was found to be EPR silent, indicating that the Cu^{II} ions in the μ-thiolate complex are antiferromagnetically coupled. In the NMR spectrum the signals are relatively broad, most likely because of paramagnetic impurities or partial population of the S = 1 spin state at room temperature. Using Evans' method we found the magnetic moment in CD_2Cl_2 to be μ_{eff} = 1.05 μ_B, a value which is significantly lower than the spin-only value (2.83 μ_B for a dinuclear complex) supporting the antiferromagnetic coupling.[32,33] The NMR spectrum of the same complex mixture in CD_3CN shows small downfield shifts compared to the spectrum of the free ligand and reveals splitting of the H-8 and H-9 proton peaks, both features indicating coordination of copper to the ligand. The diamagnetic nature of the compound in acetonitrile and the absence of d–d transitions indicate that

dx.doi.org/10.1021/ic501060w | Inorg. Chem. 2014, 53, 8494–8504

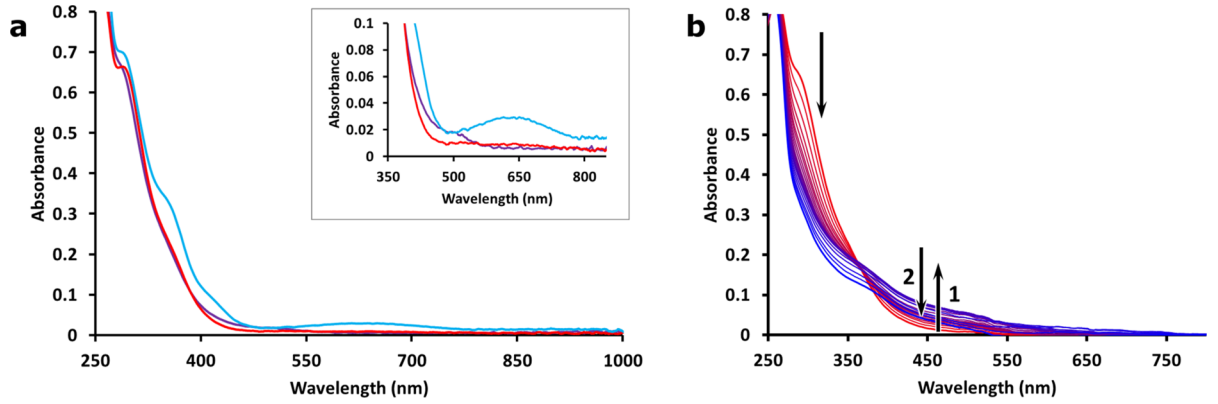

Figure 5. UV−vis spectra of $[Cu^{II}_2(L^4S)_2]^{2+}$ (a) in different solvents, MeOH (purple), CH_3CN (red), and dichloromethane (blue), and (b) at 67 °C for 21 h in MeOH at 1 mM [Cu] concentration under argon recorded with a transmission dip probe with a path length of 1.2 mm. Inset shows the same spectra zoomed in at the d−d transition band at 640 nm. The arrows show the development of the spectra over time.

the complex may be formulated as $[Cu^{I}_2(L^2SSL^2)]^{2+}$. Thus, upon addition of $[Cu^{I}(CH_3CN)_4]^{+}$ to L^2SSL^2 in acetonitrile (a polar and coordinating solvent), a Cu^{I} disulfide complex is formed, whereas in dichloromethane and acetone (less polar and weakly coordinating solvents) with the same ligand the Cu^{II} μ-thiolate complex is formed preferentially. Similar behavior with a slightly different ligand has been reported, but this was not thoroughly analyzed.[26] Addition of small amounts of acetonitrile to a solution of $[Cu^{II}_2(L^2S)_2]^{2+}$ in dichloromethane results in a gradual conversion of the Cu^{II} compound to the Cu^{I} disulfide complex, as monitored with UV−vis spectroscopy (Supporting Information Figure S9). These results suggest that in solvents of moderate coordinating properties and/or polarity a mixture of both Cu^{I} disulfide and Cu^{II} μ-thiolate species might be present.

Indeed, in methanol a mixture of both the Cu^{II} μ-thiolate and Cu^{I} disulfide compound was observed, as shown with UV−vis spectroscopy (Figure 4a). Cooling of such a methanolic solution down to 243 K resulted in an increase in the intensity of the d−d transitions and the Cu^{II} ← S LMCT characteristic for the Cu^{II} μ-thiolate species. When allowing the solution to warm to room temperature after cooling, we see that this conversion is reversible (red dots, Figure 4b). Similar results were obtained when the conversion was measured with ^{1}H NMR spectroscopy, as shown in Supporting Information Figure S2. When the solution was heated up to 333 K the d−d transitions and Cu^{II} ← S LMCT became lower in intensity over time, indicating an increase in Cu^{I} disulfide concentration. A plot of the absorbance at 358 nm versus time is shown in Figure 4c. When the solution is cooled down to room temperature after heating, there was no increase in the d−d transitions and Cu^{II} ← S LMCT, indicating no conversion back to the Cu^{II} μ-thiolate species. Heating the solution for a longer time does not result in further changes in the spectrum. These results show that the Cu^{I} disulfide−Cu^{II} μ-thiolate equilibrium is temperature dependent and reversible at lower temperatures, but not at temperatures above room temperature.

With L^4SSL^4 a different situation was observed. When $[Cu^{I}(CH_3CN)_4]^{+}$ is added to L^4SSL^4 in methanol a green solution is obtained, with UV−vis absorption bands similar to the bands of $[Cu^{II}_2(L^2S)_2]^{2+}$ in dichloromethane: the π^* ← π transition of the pyridyl groups at 261 nm (ε = 8350 M^{-1} cm^{-1}), Cu^{II} ← S LMCT transitions at 291 nm (ε = 5800 M^{-1} cm^{-1}) and 345 nm (ε = 2900 M^{-1} cm^{-1}), a d−d transition at 616 nm (ε = 245 M^{-1} cm^{-1}), and finally one band at 415 nm (ε = 800 M^{-1} cm^{-1}) that can be ascribed to either another LMCT or d−d transition. On the basis of the similarities of this UV−vis spectrum with that of $[Cu^{II}_2(L^2S)_2]^{2+}$, the complex in methanol is most likely the Cu^{II} μ-thiolate compound $[Cu^{II}_2(L^4S)_2]^{2+}$. The UV−vis spectrum of this complex was found to depend on the solvent (Figure 5a), suggesting that varying amounts of the μ-dithiolate compound $[Cu^{II}_2(L^4S)_2]^{2+}$ and of the disulfide compound $[Cu^{I}_2(L^4SSL^4)]^{2+}$ may be present in different solvents, an effect that was recently reported for ligand L^1SSL^1 and that we also see for L^2SSL^2.[16] The ^{1}H NMR spectrum of $[Cu^{II}_2(L^4S)_2]^{2+}$ in CD_3OD shows broad peaks in the diamagnetic region (Supporting Information Figure S4). Using the Evans' method we found the magnetic moment μ_{eff} in CD_3OD to be 3.80 μ_B. This value implies that the complex is paramagnetic, which could mean that the antiferromagnetic coupling is very weak due to steric interactions resulting in a longer Cu−Cu distance in the complex. Another explanation is that in solution the complex forms monomer or oligomers instead of dimers resulting in the disappearance of the antiferromagnetic coupling. When the green methanolic solution containing $[Cu^{II}_2(L^4S)_2]^{2+}$ was heated to reflux temperature for a period of ∼30 h, a brown solution was formed, from which crystals of $[Cu^{I}_2(L^4SSL^4)](BF_4)_2$ (section 2.2) were obtained. The conversion from $[Cu^{II}_2(L^4S)_2]^{2+}$ to $[Cu^{I}_2(L^4SSL^4)]^{2+}$ was monitored using UV−vis spectroscopy (Figure 5b). Upon heating, the Cu ← S LMCT transition at 345 nm shifted to 297 nm (ε = 2300 M^{-1} cm^{-1}) and became less intense over time. The absence of an isosbestic point indicated formation of an intermediate species in going from $[Cu^{II}_2(L^4S)_2]^{2+}$ to $[Cu^{I}_2(L^4SSL^4)]^{2+}$; the formation of this intermediate is indicated by the arrows in Figure 5b. The conversion was also monitored by ^{1}H NMR spectroscopy. This showed the disappearance of $[Cu^{II}_2(L^4S)_2]^{2+}$ over time and the appearance of very low intensity diamagnetic peaks that can possibly be ascribed to $[Cu^{I}_2(L^4SSL^4)]^{2+}$ (Supporting Information Figure S5). The low intensity of the peaks might indicate the presence of paramagnetic species. However, the relatively broad signals obtained for the complexes with L^4SSL^4 may arise from the presence of a mixture of diastereoisomers. Thus, in contrast with $[Cu^{II}_2(L^2S)_2]^{2+}$, $[Cu^{II}_2(L^4S)_2]^{2+}$ is found to be a kinetic, less stable product that can convert to $[Cu^{I}_2(L^4SSL^4)]^{2+}$.

Cyclic voltammetry was carried out for $[Cu^{II}_2(L^2S)_2]^{2+}$, $[Cu^{II}_2(L^4S)_2]^{2+}$, $[Cu^{I}_2(L^2SSL^2)]^{2+}$, and $[Cu^{I}_2(L^4SSL^4)]^{2+}$ (Supporting Information Figures S10 and S11). All complexes show

dx.doi.org/10.1021/ic501060w | Inorg. Chem. 2014, 53, 8494−8504

Table 2. Energies of Formation (kJ mol^{-1}) of Cu^{II} μ-Thiolate (A) and Cu^{I} Disulfide (B or C) Complexes for Different LSSL Ligands and 2 $[Cu(CH_3CN)_4]^+$ in Acetonitrile[a]

	 A	 B	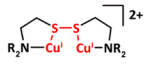 C	$\Delta\Delta E = \Delta E_B - \Delta E_A$[b]	$\Delta\Delta E = \Delta E_C - \Delta E_A$[b]
L^1SSL^1	–80	**–83**	–73	–4 (–3)	7 (9)
L^2SSL^2	–73	**–86**	–83	–13 (–11)	–9 (–4)
L^3SSL^3	–63	**–102**	–97	–39 (–35)	–34 (–27)
L^4SSL^4	–44	–60	**–93**	–16 (–11)	–49 (–32)
L^5SSL^5	27	–20	**–83**	–47 (–41)	–110 (–99)

[a]See eq 1. Computed at ZORA-OPBE/TZ2P in CH_3CN (COSMO). [b]The energy differences in parentheses are the Gibbs free energies, $\Delta\Delta G$ (kJ mol^{-1}).

multiple irreversible waves, making assignment of the peaks difficult.

2.4. DFT Calculations. *2.4.1. Energy of Formation.* The formation of a Cu^{II} μ-thiolate complex (**A**) and a Cu^{I} disulfide complex (**B** or **C**) was studied computationally with DFT, calculating the energies for the different geometries for copper compounds of the ligands depicted in Figure 1. The Cu^{II} ions in the Cu^{II} μ-thiolate species are antiferromagnetically coupled,[16,27] which has been taken into account computationally (see section 5.3). The energy of formation was calculated according to eq 1, and these values are given in Table 2.

$$\mathbf{LSSL} + 2[Cu^{I}(CH_3CN)_4]^+ \rightarrow [Cu_2(\mathbf{LSSL})]^{2+} \text{ or } [Cu_2(\mathbf{LS})_2]^{2+} + 8CH_3CN \quad (1)$$

The computational results corroborate the trends that are witnessed experimentally for the reaction of different ligands with Cu^{I}. A lower energy was found for the Cu^{I} disulfide in transoid conformation **B** for L^1SSL^1, L^2SSL^2, and L^3SSL^3, while for L^4SSL^4 and L^5SSL^5 the cisoid conformation **C** was found to have a lower energy. These results are in agreement with the crystal structures reported for $[Cu^{I}_2(L^3SSL^3)]^{2+}$ and $[Cu^{I}_2(L^5SSL^5)]^{2+}$.[27] When comparing the energy difference, $\Delta\Delta E$, between structure **A** and the most stable Cu^{I} disulfide structure for each ligand, an increase of $\Delta\Delta E$ was observed following the series L^1SSL^1, L^2SSL^2, and L^3SSL^3, i.e., when the number of *ortho*-methyl groups increased from zero to four. L^1SSL^1, which has been reported to form a Cu^{II} μ-thiolate complex, shows an almost negligible energy difference (−4 kJ mol^{-1}). This energy difference is in the order of the accuracy that can be obtained with our methodology. $\Delta\Delta E$ was found to be larger between **A** and **C** for L^4SSL^4 and L^5SSL^5, −49 kJ mol^{-1} and −110 kJ mol^{-1}, respectively. For L^4SSL^4 the energy difference between **A** and **C** was found to be of a similar magnitude as the energy of formation of **A** (−44 kJ mol^{-1}), showing that the Cu^{II} μ-thiolate complex is intermediary in its formation energy between the starting point (L^4SSL^4 + 2 $[Cu(CH_3CN)_4]^+$) and the Cu^{I} disulfide species. The formation of **A** appears even to be unfavorable for L^5SSL^5 (+27 kJ mol^{-1}) which leads to a large energy difference between **A** and **C**. For L^2SSL^2 and L^4SSL^4 three different geometries were calculated for the μ-thiolate species **A**, as a result of the asymmetry caused by the pyridyl groups (Supporting Information Figures S12 and S13); only the energy of the complexes with the lowest energy are given in Table 2. The computed global minimum for $[Cu^{II}_2(L^2S)_2]^{2+}$ was found to have the same conformation as that found in the X-ray crystal structure (Figure 2).

The differences in Gibbs energy, $\Delta\Delta G$, between **A** and **B** or **A** and **C** are somewhat smaller than $\Delta\Delta E$, but the general trends are the same. The energies of formation in the gas phase show similar trends (Supporting Information Tables S4 and S5).

No computational evidence was found for coordination of acetonitrile to Cu^{II} μ-thiolate or Cu^{I} disulfide complexes. This was established by bringing an acetonitrile molecule in close vicinity (coordination distance) of the copper center and calculating whether it would coordinate to the metal center. This in silico experiment was done for $[Cu^{II}_2(L^2S)_2]^{2+}$, $[Cu^{II}_2(L^4S)_2]^{2+}$, $[Cu^{I}_2(L^2SSL^2)]^{2+}$ (conformation **B**), and $[Cu^{I}_2(L^4SSL^4)]^{2+}$ (conformation **C**), and in all cases the acetonitrile molecule moved away from the copper complex. Dissociation of one of the pyridyl groups to allow the coordination of acetonitrile was suggested for $[Cu^{I}$(tris(2-pyridylmethyl)amine)$]^+$ by Karlin and co-workers.[34] To see whether this is the case for our complexes, we calculated the energies for **A**, **B**, and **C** for all five ligands with one dissociated pyridyl group and one CH_3CN molecule per copper ion. These calculations show that dissociation of the pyridyl groups in favor of an acetonitrile molecule is in all cases less favorable compared to its analogue without coordinated CH_3CN (Supporting Information Table S6). Furthermore, the dissociation of the S atom in the Cu^{I} complexes in favor of CH_3CN has been calculated for all ligands and again is shown to be less favorable compared to no coordination of acetonitrile. These experiments indicate that the solvent-induced interconversion between the Cu^{II} μ-thiolate and Cu^{I} disulfide species are likely due to polarity differences rather than coordination of the solvent.

2.4.2. Bonding Energy. To gain more insight as to *why* either the μ-thiolate or the disulfide complex forms, the bond energy ΔE_{bond} between the two Cu^{I} ions and the different ligands was analyzed in more detail in the gas phase. Note that the key trends found for the condensed phase computations also occur in the gas phase; that is, the thiolate (**A**) and the disulfide forms (**B** or **C**) are essentially at the same energy for L^1SSL^1 whereas the disulfide form is clearly more stable for the other ligands. The ΔE_{bond} comprises the deformation energy of the ligand (ΔE_L), the electrostatic repulsion between the two Cu^{I} ions (ΔE_{Cu-Cu}), and the copper−ligand interaction energy (ΔE_{int}).

$$\Delta E_{bond} = \Delta E_L + \Delta E_{Cu-Cu} + \Delta E_{int} \quad (2)$$

ΔE_L is the strain energy that is needed to distort the ligand from its lowest energy conformation to the conformation in the complex. The ΔE_{Cu-Cu} represents the energy that is needed to

dx.doi.org/10.1021/ic501060w | Inorg. Chem. 2014, 53, 8494−8504

Table 3. Ligand Distortion Energy (ΔE_L), Cu^I–Cu^I Electrostatic Repulsion Energy (ΔE_{Cu-Cu}), Interaction Energy (ΔE_{int}), and Bonding Energy (ΔE_{bond}) in kJ mol^{-1} for Complexes with Geometry A, B, and C in the Gas Phase[a]

	A				B				C			
	ΔE_L[b]	ΔE_{Cu-Cu}	ΔE_{int}	ΔE_{bond}	ΔE_L	ΔE_{Cu-Cu}	ΔE_{int}	ΔE_{bond}	ΔE_L	ΔE_{Cu-Cu}	ΔE_{int}	ΔE_{bond}
L^1SSL^1	400	1854	−3161	−907	119	1730	−2772	−923	128	1724	−2774	−922
L^2SSL^2	374	1849	−3140	−917	100	1728	−2772	−944	101	1717	−2767	−949
L^3SSL^3	376	1841	−3113	−897	104	1727	−2773	−942	105	1718	−2767	−944
L^4SSL^4	448	1855	−3197	−894	165	1724	−2781	−893	146	1725	−2793	−922
L^5SSL^5	487	1842	−3163	−835	200	1720	−2783	−863	156	1727	−2810	−927

[a]Computed at ZORA-OPBE/TZ2P. [b]The deformed ligand was computed as a singlet biradical (see section 5.3).

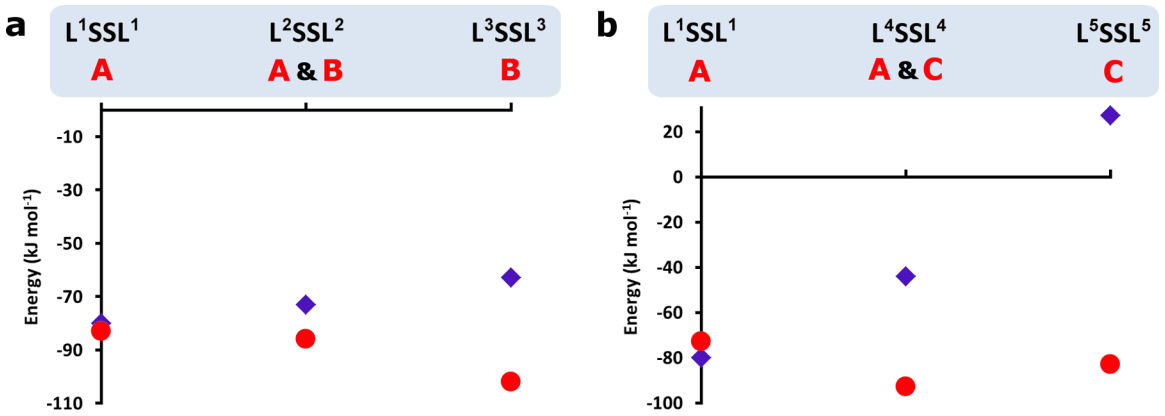

Figure 6. Plot of the formation energies (kJ mol^{-1}) of the μ-thiolato Cu^{II} (blue diamonds) and Cu^I disulfide (red circles) species (a) for ligands L^1SSL^1, L^2SSL^2, and L^3SSL^3 (conformation A and B) and (b) for ligands L^1SSL^1, L^4SSL^4, and L^5SSL^5 (conformation **A** and **C**). The red letters indicate the conformation found experimentally for each ligand.

bring the two Cu^I ions from infinity to the distance that they have in the complex. The ΔE_{int} accounts for the interaction energy between the deformed ligand and the fragment of two Cu^I ions. The results are given in Table 3.

The values for ΔE_L show that the energy it takes to change the ligand to the complex conformation is much higher for the μ-thiolate complexes than for the disulfide complexes **B** and **C**. The reason for this is that in the thiolate complex **A** the S–S bond is broken, whereas in the disulfide complexes **B** and **C** it is preserved. ΔE_{bond} differs slightly for ligands L^1SSL^1, L^2SSL^2, and L^3SSL^3 in conformation **A** and shows only small energy differences between geometries **B** and **C**.

For L^4SSL^4 and L^5SSL^5, a large increase for ΔE_L is observed for **A**, leading to somewhat less stabilizing ΔE_{bond} values of −894 and −835 kJ mol^{-1}, respectively. For **B** and **C** a similar trend can be seen with significantly more destabilizing ligand strain energy ΔE_L in combination with slightly more stabilizing ΔE_{int} values. This indicates that the energy necessary to distort L^4SSL^4 and L^5SSL^5 to the binding conformation is much larger than for L^1SSL^1, L^2SSL^2, and L^3SSL^3. The electrostatic repulsion ΔE_{Cu-Cu} between the two copper ions is nearly constant going down the column from L^1SSL^1 to L^5SSL^5, showing that complex formation is predominantly dependent on the ligand deformation. The ΔE_L values for L^4SSL^4 and L^5SSL^5 also reveal a large preference for the formation of geometry **C** over **B**.

3. DISCUSSION

Two new ligands L^2SSL^2 and L^4SSL^4 were synthesized with structural properties intermediate to those of ligand L^1SSL^1 and L^3SSL^3 or L^5SSL^5, respectively. When these ligands are reacted with $[Cu(CH_3CN)_4]^+$ in solution, either a Cu^{II} μ-thiolate (**A**) or a Cu^I disulfide (transoid **B** or cisoid **C**) species is formed depending on the structure of the ligand, the coordinating properties of the solvent, and the temperature. For the ligand L^2SSL^2, the formation of **A** is confirmed by X-ray structure determination of $[Cu^{II}_2(L^2S)_2](BF_4)_2{\cdot}C_3H_6O$, and is further characterized by its specific LMCT and d–d transitions in the UV–vis spectrum. For the ligand L^4SSL^4, the formation of $[Cu^I_2(L^4SSL^4)]^{2+}$ was determined by X-ray crystallography, which confirms the **C** geometry of $[Cu^I_2(L^4SSL^4)]^{2+}$. For comparison, single crystals of $[Cu^I_2(L^3SSL^3)](BF_4)_2$ were also prepared; X-ray structure determination showed the transoid-disulfide conformation **B** (see Supporting Information) to be in agreement with an earlier report.[27]

Modeling these systems computationally with DFT is challenging because of the large number of atoms, but the calculations and the experimental facts give a consistent view. The formation energies calculated for the different copper compounds using DFT show clear trends in the two ligand series, which have been plotted in Figure 6. When the geometry optimizations are done in the gas phase, similar trends are obtained (Supporting Information Tables S4 and S5), indicating that these energies are not strongly dependent on the solvent, but are inherent to the system. For L^1SSL^1, the

dx.doi.org/10.1021/ic501060w | Inorg. Chem. 2014, 53, 8494–8504

energy difference between the Cu^{II} thiolate species and the Cu^{I} disulfide complex is very small, but with increasing steric bulk (methyl groups) or increasing number of ethylene bridges (between the tripodal amine and the pyridine rings) on the ligand the energy differences become larger. The presence of an ethylene bridge seems to destabilize the Cu^{II} μ-thiolate species to a greater extent than the introduction of a methyl group on the pyridyl ring. This is to be expected considering that the methylene-bridged ligands, like $\mathbf{L^1SSL^1}$, form five-membered chelate rings with copper whereas the ethylene-bridged ligands, like $\mathbf{L^5SSL^5}$, form six-membered chelate rings with copper (Figure 7). In the μ-thiolate compounds, the Cu^{II} ions have

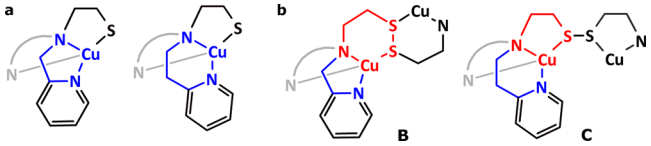

Figure 7. Schematic representation of the five- and six-membered rings formed by copper and the pyridyl groups in blue (a) and the five- and six-membered rings formed by copper and the disulfide bridge in geometry **B** and **C** in red (b).

square-pyramidal geometries and therefore prefer coordination angles close to 90°, which means that they would prefer a five-membered chelate ring over a six-membered ring. The larger Cu^{I} ions prefer tetrahedral geometries and can therefore also cope with larger coordination angles such as those found in a six-membered chelate ring. Considering this, it is not surprising that $\mathbf{L^5SSL^5}$ and to some extent $\mathbf{L^4SSL^4}$ form Cu^{I} disulfide compounds in conformation **C**, which is also reflected in ΔE_L (Table 3). The deformation energy of the ligand is much higher for $\mathbf{L^4SSL^4}$ and for $\mathbf{L^5SSL^5}$ than it is for the other three ligands indicating that formation of either **A** or **C** is largely induced by steric effects, i.e., the preference of Cu^{I} and Cu^{II} to form six- and five-membered rings in combination with the length of the ethylene versus methylene bridges in the ligands. In this respect, $\mathbf{L^4SSL^4}$ is a unique ligand with its ability to form both five-membered and six-membered rings, ultimately leading to the Cu^{I} disulfide conformation **C**, but with the ability to also form the Cu^{II} μ-thiolato complex.

A novel discovery is that the equilibrium between the Cu^{II} μ-thiolate and the Cu^{I} disulfide species can be temperature-dependent. $\mathbf{L^2SSL^2}$ favors formation of the μ-thiolate complex at low temperatures and the disulfide compound at higher temperatures, although it must be noted that this equilibrium is only reversible below room temperature. Whether the compound $[Cu^{I}_2(\mathbf{L^2SSL^2})]^{2+}$ adopts conformation **B** and/or **C** is rather difficult to determine. As far as we know, clear spectroscopic differences between these two coordination isomers do not exist. Since $\mathbf{L^2SSL^2}$ is similar to $\mathbf{L^3SSL^3}$, which has been crystallized with Cu^{I} in geometry **B**,[27] it would not be surprising if $\mathbf{L^2SSL^2}$ gives the same conformation as confirmed by the energies calculated for the complexes of $\mathbf{L^2SSL^2}$ that indicate a slight preference for geometry **B** (Table 2).

The UV−vis absorption spectra of $[Cu^{II}_2(\mathbf{L^4S})_2]^{2+}$ show varying absorption intensities in different solvents (Figure 5a). A similar effect was recently reported by the group of Stack who studied the interaction of Cu^{I} with the ligand $\mathbf{L^1SSL^1}$, which they ascribed to the formation of a higher concentration of μ-thiolate species **A** in less coordinating solvents.[16] In the temperature-controlled conversion of $[Cu^{II}_2(\mathbf{L^4S})_2]$ to $[Cu^{I}_2(\mathbf{L^4SSL^4})]^{2+}$, the formation of an intermediate species was observed, which may be ascribed to the intermediate formation of conformation **B** before isomerization to **C** occurs. This is in agreement with the DFT results, showing that geometry **B** with −60 kJ mol^{-1} is in between geometry **A** (−44 kJ mol^{-1}) and geometry **C** (−93 kJ mol^{-1}) in terms of formation energy. Since there is no evidence of the reverse reaction from **C** to **A**, the μ-thiolato Cu^{II} species **A** can be described as a kinetic product and the Cu^{I} disulfide species **C** as the thermodynamic product. A schematic overview of the experimental results is provided in Figure 8.

Considering the results from both the experiments and the calculations, it seems that whether the Cu^{II} μ-thiolate species forms largely depends on the activation barrier in going from **A** to **B** or **C**. For $\mathbf{L^2SSL^2}$ this barrier appears to be low, which makes studying the equilibrium in methanol possible. In contrast, for $\mathbf{L^4SSL^4}$ this barrier is high, resulting in initial formation of conformation **A**, which can be irreversibly converted to **C** by heating. Future work will be directed to quantifying these activation barriers, which is even more

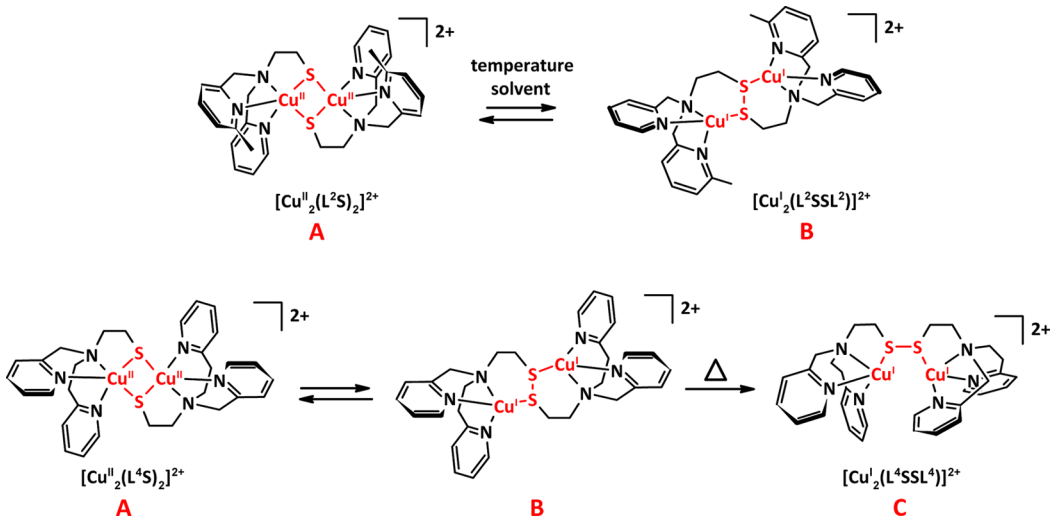

Figure 8. Schematic representation of the formation of Cu^{II} μ-thiolato and Cu^{I} disulfide complexes with $\mathbf{L^2SSL^2}$ and $\mathbf{L^4SSL^4}$.

dx.doi.org/10.1021/ic501060w | Inorg. Chem. 2014, 53, 8494−8504

challenging. This might provide important additional information concerning this biologically highly relevant equilibrium.

4. CONCLUSION

Two new dissymmetric ligands, $\mathbf{L^2SSL^2}$ and $\mathbf{L^4SSL^4}$, were synthesized with an intermediate number of methyl groups ($\mathbf{L^2SSL^2}$) or ethyl bridges ($\mathbf{L^4SSL^4}$) compared with the known ligands $\mathbf{L^1SSL^1}$, $\mathbf{L^3SSL^3}$, and $\mathbf{L^5SSL^5}$. Their Cu^{II} μ-thiolate and Cu^{I} disulfide complexes were characterized in the solid state or in solution. For $\mathbf{L^2SSL^2}$ the two redox isomeric forms are shown to be in an equilibrium that depends both on temperature and on solvent. The behavior of $\mathbf{L^4SSL^4}$ is unique as it forms the Cu^{II} μ-thiolate species as the kinetic product and the Cu^{I} disulfide complex as the thermodynamic product in methanol. These ligands opened the unique opportunity to compare both Cu^{II} μ-thiolate and Cu^{I} disulfide complexes in the same experimental conditions. DFT calculations provide theoretical insight into the energies involved in the formation of Cu^{II} μ-thiolate and Cu^{I} disulfide complexes and yield a picture that is consistent with the experimental results. An increase in energy difference between the Cu^{II} μ-thiolate and the Cu^{I} disulfide species was observed with increasing steric bulk (methyl groups) or increasing number of ethylene bridges (between the tripodal amine and the pyridine rings) on the ligands. This implies that deformation of the ligand from its equilibrium structure to the geometry in the complex plays a large role as to whether the Cu^{II} μ-thiolate complex forms. The equilibrium between the two redox-isomeric species seems to be largely dependent on the activation barrier of going from the thiolate to the disulfide complex. This information provides interesting opportunities for future research as proteins generally use low activation barriers for their catalytic electron transfer reactions. Besides this, control over this biomimetic redox equilibrium allows for further analysis and understanding of biological copper−sulfur reactions and might provide opportunities in the field of electron sources and sinks.

5. EXPERIMENTAL SECTION

5.1. General Methods. Reagents and solvents were obtained from commercial sources. The syntheses of all copper complexes were carried out using standard Schlenk-line techniques under an argon atmosphere. Solvents were distilled and deoxygenated by bubbling a stream of argon through the solution and stored on activated molecular sieves under argon prior to use. $[Cu^{I}(CH_3CN)_4](BF_4)$, $[Cu^{I}(CH_3CN)_4](ClO_4)$, and bis(2-(*N*-pyridylmethyl)aminoethyl) disulfide were synthesized according to literature procedures.[25] ^1H and ^{13}C NMR spectra were recorded on a Bruker 300 DPX spectrometer. NMR experiments under argon were carried out using a J. Young NMR tube. The Evans method was carried out with mesitylene as the reference compound. IR spectra were obtained on a Perkin-Elmer UATR (Single Reflection Diamond) Spectrum Two device (4000−700 cm^{-1}; resolution 4 cm^{-1}). Mass spectrometry was measured using a Finnigan Aqua Mass Spectrometer (MS) with electrospray ionization (ESI). Sample introduction was achieved through a Dionex ASI-100 automated sample injector with an eluent flow rate of 0.2 mL/min. UV−vis spectra were collected using a transmission dip probe with variable path length on an Avantes Avaspec-2048 spectrometer with Avalight-DH-S-BAL light source. Elemental analyses were performed by the Microanalytical laboratory Kolbe in Germany. Cyclic voltammetry was performed with an Autolab PGstat10 potentiostat controlled by GPES4 software. A three electrode arrangement with a glassy carbon working electrode (3 mm diameter), an Ag/AgCl double junction reference electrode, and a Pt wire counter electrode were used in different solvents with 0.1 M NBu_4PF_6 as the electrolyte. In these conditions the Fc/Fc^+ couple was found to be located at +417 mV in MeOH, with a peak-to-peak separation of 51 mV; at +461 mV in dichloromethane, with a peak-to-peak separation of 92 mV; at +433 mV in acetonitrile, with a peak-to-peak separation of 51 mV. Potentials are given relative to the Ag/AgCl electrode.

5.2. X-ray Crystallography. *5.2.1. $[Cu^{II}_2(L^2S)_2](BF_4)_2\cdot C_3H_6O$.* All reflection intensities for $[Cu^{II}_2(\mathbf{L^2S})_2](BF_4)_2\cdot C_3H_6O$ were measured at 110(2) K using a SuperNova diffractometer (equipped with Atlas detector) with Cu Kα radiation (λ = 1.541 78 Å) under the program CrysAlisPro (Version 1.171.36.24 Agilent Technologies, 2012). The program CrysAlisPro was also used to refine the cell dimensions and for data reduction. The structure was solved with the program SHELXS-2013 (Sheldrick, 2013)[35] and was refined on F^2 with SHELXL-2013 (Sheldrick, 2013).[35] Analytical numeric absorption corrections based on a multifaceted crystal model were applied using CrysAlisPro. The temperature of the data collection was controlled using the system Cryojet (manufactured by Oxford Instruments). The H atoms were placed at calculated positions using the instructions AFIX 23, AFIX 43, or AFIX 137 with isotropic displacement parameters having values 1.2 or 1.5 times U_{eq} of the attached C atoms.

5.2.2. $[Cu^{I}_2(L^4SSL^4)](BF_4)_2$. All reflection intensities for $[Cu^{I}_2(\mathbf{L^4SSL^4})](BF_4)_2$ were measured at 110(2) K using a KM4/Xcalibur (detector: Sapphire3) with enhanced graphite-monochromated Mo Kα radiation (λ = 0.710 73 Å) under the program CrysAlisPro (Version 1.171.35.11 Oxford Diffraction Ltd., 2011). The program CrysAlisPro was used to refine the cell dimensions and for data reduction. The structure was solved with the program SHELXS-97 (Sheldrick, 2008)[35] and was refined on F^2 with SHELXL-97 (Sheldrick, 2008).[35] Analytical numeric absorption corrections based on a multifaceted crystal model were applied using CrysAlisPro. The temperature of the data collection was controlled using the system Cryojet (manufactured by Oxford Instruments). The H atoms were placed at calculated positions using the instructions AFIX 23 or AFIX 43 with isotropic displacement parameters having values 1.2 times U_{eq} of the attached C atoms.

5.3. DFT Calculations. All calculations were performed with the Amsterdam Density Functional (ADF) program,[36,37] using relativistic DFT at ZORA OPBE/TZ2P for geometry optimization and energies.[38] Solvation in acetonitrile was simulated using the conductor-like screening model (COSMO).[39−42] All stationary points in the gas phase and in the condensed phase were verified to be minima on the potential energy surface (PES) through vibrational analysis. The energies of the singlet state of the Cu^{II} μ-thiolate complexes (E^S) have been obtained from the unrestricted broken-symmetry singlet energies (E^{BS}) and the energy of the triplet (E^T) with the approximate projection method of Noodleman: $E^S = 2E^{BS} - E^T$.[43,44] The biradical singlet state of the deformed ligand with the elongated S−S bond has also been obtained in this way.

The Gibbs free energies ($\Delta G = \Delta H - T\Delta S$) were evaluated with the following procedure. Enthalpies at 298.15 K and 1 atm (ΔH_{298}) were calculated from electronic bond energies (ΔE) in the solvent and vibrational frequencies using standard thermochemistry relations for an ideal gas, according to[45]

$$\Delta H_{298} = \Delta E + \Delta E_{trans,298} + \Delta E_{rot,298} + \Delta E_{vib,0} + \Delta(\Delta E_{vib,0})_{298} + \Delta(pV)$$

Here, $\Delta E_{trans,298}$, $\Delta E_{rot,298}$, and $\Delta E_{vib,0}$ are the differences between the two complexes in translational, rotational, and zero point vibrational energy, respectively; $\Delta(\Delta E_{vib,0})_{298}$ is the change in the vibrational energy difference as one goes from 0 to 298.15 K. The vibrational energy corrections are based on our frequency calculations in the gas phase. The molar work term $\Delta(pV)$ is $(\Delta n)RT$, with $n = 0$; thermal corrections for the electronic energy are neglected. The entropy ΔS was also obtained from the gas phase calculations.

Most systems were optimized in C_2 symmetry (see Supporting Information). CH_3CN was optimized with C_{3v} symmetry.

5.4. Ligand Synthesis. *5.4.1. L^2SSL^2.* Bis-2-((2-pyridylmethyl)-amino)ethyl disulfide (2.86 g, 8.55 mmol) was dissolved in methanol (20 mL). 6-Methylpyridine-2-carboxaldehyde (2.08 g, 17.1 mmol) dissolved in methanol (22.5 mL) was added, followed by a scoop of

dx.doi.org/10.1021/ic501060w | Inorg. Chem. 2014, 53, 8494−8504

anhydrous $MgSO_4$ and a few drops of formic acid. The resulting yellow solution was stirred for 4.5 h at RT. $NaCNBH_3$ (1.19 g, 18.8 mmol) was added in small portions over the course of 1 h, after which the solution was stirred for 30 min. The solution was filtered and evaporated to dryness. The product was treated with 2 M NaOH (120 mL) and extracted with dichloromethane. The organic layer was dried over $MgSO_4$ and evaporated to dryness yielding a dark yellow oil (4.05 g, 87%). The compound was purified by column chromatography over basic alumina (60/40 EtOAc/petroleum ether) yielding a cream-colored solid (0.71 g, 1.3 mmol, 16%), which can be recrystallized from petroleum ether. ^{1}H NMR (300 MHz, CD_3CN, RT): δ 2.44 (s, 6H, Py−CH_3), 2.77 (m, 8H, S−CH_2−CH_2), 3.72 (s, 4H, Py−CH_2−N), 3.76 (s, 4H, Py−CH_2−N), 7.04 (d, J = 8 Hz, 2H, Py_{Me}−H_3), 7.17 (m, 2H, Py_{Me}−H_5), 7.32 (d, J = 8 Hz, 2H, Py−H_3), 7.55 (m, 4H, Py−H_4; Py_{Me}−H_4), 7.68 (td, J = 8 Hz, 2 Hz, 2H, Py−H_5), 8.45 (m, 2H, Py−H_6). ^{13}C NMR (75 MHz, CD_3CN, RT): δ 24.5 (Py−CH_3), 37.3 (S−CH_2), 54.2 (S−CH_2−CH_2), 60.9 (Py−CH_2−N), 60.9 (Py−CH_2−N), 120.8 (Py_{Me}−C_5), 122.3 (Py_{Me}−C_3), 123.0 (Py−C_5), 124.0 (Py−C_3), 137.4 (Py_{Me}−C_4), 137.7 (Py−C_4), 149.7 (Py−C_6), 158.4 (Py_{Me}−C_2), 159.8 (Py_{Me}−C_6), 160.5 (Py−C_2). ESI-MS found (calculated) for $[M + H]^+$ m/z 545.1 (545.3). IR (neat, cm^{-1}): 2817m, 1591s, 1578s, 1463s, 1436s, 1360s, 1107s, 788m, 762m, 614s.

5.4.2. L^4SSL^4. To bis-2-((2-pyridylmethyl)amino)ethyl disulfide (6.24 g, 18.7 mmol) was added glacial acetic acid (3.0 mL, 52.0 mmol), 2-vinylpyridine (5.2 mL, 48.0 mmol), and 8 mL of methanol. The solution was stirred for 4 days at 70 °C and then evaporated to dryness yielding a dark green oil. To this oil a solution of Na_2CO_3 (100 mL, 2 M) was added, and the aqueous mixture was extracted with dichloromethane (3 × 100 mL). The combined layers were dried over Na_2SO_4 and evaporated to dryness giving a dark brown oil. This product was purified by column chromatography over basic alumina (60−70% EtOAc/petroleum ether) yielding a light-brown oil (6.63 g, 12.2 mmol, 65%). ^{1}H NMR (300 MHz, CD_3OD, RT): δ 2.75 (m, 4H, S−CH_2), 2.85 (m, 4H, S-CH_2−CH_2), 2.92 (m, 8H, Py−CH_2−CH_2−N), 3.79 (s, 4H, Py−CH_2−N), 7.23 (m, 4H, Py−H_3), 7.29 (d, J = 8 Hz, 2H, Py−H_5), 7.35 (d, J = 8 Hz, 2H, Py−H_5), 7.69 (m, 4H, Py−H_4), 8.39 (m, 4H, Py−H_6). ^{13}C NMR (75 MHz, CD_3OD, RT): δ 36.5 (Py−CH_2−CH_2−N), 37.3 (S−CH_2), 54.5 (S−CH_2−CH_2), 55.4 (Py−CH_2−CH_2−N), 60.7 (Py−CH_2−N), 122.9 (Py−C_3), 123.7 (Py−C_3), 124.8 (Py−C_5), 125.5 (Py−C_5), 138.5 (Py−C_4), 149.2 (Py−C_6), 149.6 (Py−C_6), 160.8 (Py−C_2), 161.4 (Py−C_2). ESI-MS found (calculated) for $[M + Na]^+$ m/z 567.1 (567.2); $[M + H]^+$ m/z 545.0 (545.3). IR (neat, cm^{-1}): 2930m, 2816m, 1589s, 1568m, 1474m, 1433s, 993m, 752s, 403m.

5.5. Complex Synthesis. *5.5.1. $[Cu^{II}_2(L^2S)_2](BF_4)_2$.* $\mathbf{L^2SSL^2}$ (68.9 mg, 0.126 mmol) was dissolved in dichloromethane (7.5 mL). To this solution was added $[Cu(CH_3CN)_4](BF_4)$ (79.8 mg, 0.253 mmol), which resulted in a very dark green solution. This solution was stirred for 1 h after which the solution was added to 80 mL of pentane resulting in a greenish blue-gray precipitate (97.7 mg, 0.116 mmol, 91%). Crystals suitable for X-ray structure determination were obtained by slow vapor diffusion of pentane into an acetone solution containing the complex. ^{1}H NMR (300 MHz, CD_2Cl_2, RT): δ 2.70 (s, 6H, Py−CH_3), 3.16 (s, 8H, S−CH_2−CH_2), 3.99 (s, 8H, Py−CH_2−N), 7.24 (t, J = 9 Hz, 4H, Py−H), 7.42 (s, 4H, Py−H), 7.71 (t, J = 7.5 Hz, 2H, Py−H), 7.82 (t, J = 7.5 Hz, 2H, Py−H), 8.59 (s, 2H, Py−H_6). ESI-MS found (calculated) for $[^1/_2M + MeOH - BF_4]^+$ m/z 367.0 (367.1). Anal. Calcd for $[Cu^{II}_2(\mathbf{L^2S})_2](BF_4)_2$: C 42.62, H 4.29, N 9.94, S 7.59. Found: C 41.95, H 4.62, N 9.99, S 7.69. The slightly high H% is likely due to the highly hygroscopic and air-sensitive nature of the compound. IR (neat, cm^{-1}): 1606s, 1577s, 1466m, 1442m, 1050vs, 786m, 520s. UV−vis in dichloromethane at 1 mM [Cu] concentration: 261 nm (ε = 17 200 M^{-1} cm^{-1}), 300 nm (ε = 7100 M^{-1} cm^{-1}), 358 nm (ε = 4200 M^{-1} cm^{-1}), 500 nm (ε = 1200 M^{-1} cm^{-1}), 627 nm (ε = 1100 M^{-1} cm^{-1}), 928 nm (ε = 410 M^{-1} cm^{-1}).

5.5.2. $[Cu^{I}_2(L^2SSL^2)](BF_4)_2$. $\mathbf{L^2SSL^2}$ (5.45 mg, 0.01 mmol) was dissolved in acetonitrile (2 mL). To this solution was added $[Cu(CH_3CN)_4](BF_4)$ (6.29 mg 0.02 mmol), resulting in a light greenish yellow solution. Attempts to isolate the complex resulted in the formation of oil. ^{1}H NMR (300 MHz, CD_3CN, RT): δ 2.57 (s, 6H, Py−CH_3), 2.90 (m, 8H, S−CH_2−CH_2), 3.81 (s, 4H, Py−CH_2−N), 3.83 (s, 4H, Py−CH_2−N), 7.17 (d, J = 8 Hz, 2H, Py_{Me}−H_3), 7.25 (d, J = 8 Hz, 2H, Py−H_3), 7.30 (m, 2H, Py_{Me}−H_4), 7.44 (d, J = 8 Hz, 2H, Py_{Me}−H_5), 7.66 (t, J = 8 Hz, 2H, Py−H_4) 7.76 (t, J = 8 Hz, 2H, Py−H_5), 8.52 (d, J = 4 Hz, 2H, Py−H_6). ^{13}C NMR (75 MHz, CD_3CN, RT): δ 26.1 (Py−CH_3), 36.8 (S−CH_2), 56.6 (S−CH_2−CH_2), 60.2 (Py−CH_2), 60.5 (Py−CH_2), 122.0 (Py_{Me}−C_5), 124.9 (Py_{Me}−C_3, Py−C_5), 125.3 (Py−C_3), 139.2 (Py_{Me}−C_4), 139.4 (Py−C_4), 150.1 (Py−C_6), 156.9 (Py_{Me}−C_2), 157.8 (Py_{Me}−C_6), 158.7 (Py_{Me}−C_2). ESI-MS found (calculated) for $[Cu_2(\mathbf{L^2SSL^2})]^{2+}$ m/z 335.1 (335.1); $[^1/_2M + MeOH - BF_4]^+$ m/z 367.0 (367.1) $[Cu(\mathbf{L^2SSL^2})]^+$ m/z 607.1 (607.2). UV−vis in acetonitrile at 1 mM [Cu] concentration: 257 nm (ε = 7950 M^{-1} cm^{-1}), 309 nm (ε = 3150 M^{-1} cm^{-1}).

5.5.3. $[Cu^{II}_2(L^4S)_2](BF_4)_2$. $\mathbf{L^4SSL^4}$ (1 equiv) was mixed with 2 equiv of $[Cu(CH_3CN)_4](BF_4)$ in methanol yielding a bright green solution. Attempts to isolate the complex resulted in the formation of oil. ^{1}H NMR (300 MHz, CD_3OD, RT): δ 2.98 (br, 8H, S−CH_2−CH_2), 3.08 (br, 8H, Py−CH_2−CH_2−N), 4.11 (br, 2H, Py−CH_2−N), 4.22 (br, 2H, Py−CH_2−N), 7.53 (m, 8H, Py−H), 7.94 (d, J = 8 Hz, 4H, Py−H), 8.40 (br, 1H, Py−H), 8.60 (m, 1H, Py−H), 8.98 (br, 2H, Py−H). ESI-MS found (calculated) for $[Cu_2(\mathbf{L^4S})_2]^{2+}$ m/z 336.1 (335.1); $[Cu(\mathbf{L^4SSL^4})]^+$ m/z 607.1 (607.2). UV−vis in dichloromethane at 1 mM [Cu] concentration: 261 nm (ε = 8350 M^{-1} cm^{-1}), 291 nm (ε = 5800 M^{-1} cm^{-1}), 345 nm (ε = 2900 M^{-1} cm^{-1}), 415 nm (ε = 800 M^{-1} cm^{-1}), 616 nm (ε = 245 M^{-1} cm^{-1}).

5.5.4. $[Cu^{I}_2(L^4SSL^4)](BF_4)_2$. $\mathbf{L^4SSL^4}$ (34.0 mg, 0.062 mmol) was dissolved in methanol (6 mL). To this solution was added $[Cu(CH_3CN)_4](BF_4)$ (39.8 mg, 0.125 mmol), which resulted in a bright green solution. The solution containing $[Cu^{II}_2(\mathbf{L^4S})_2](BF_4)_2$ was stirred for 45 h at 67 °C resulting in a brown/green solution. This solution was added to 80 mL of diethyl ether resulting in a green/brown powder (37.1 mg, 0.044 mmol, 70%). Crystals suitable for X-ray structure determination were obtained by vapor diffusion of *n*-hexane in a methanol solution containing the complex. Anal. Calcd for $[Cu^{I}_2(\mathbf{L^4SSL^4})](BF_4)_2$: C 42.62, H 4.29, N 9.94, S 7.59. Found: C 42.62, H 4.54, N 9.88, S 7.74. ESI-MS found (calculated) for $[Cu(\mathbf{L^4S})]^+$ m/z 335.0 (335.1); $[Cu(\mathbf{L^4S}) + CH_3O]^+$ m/z 366.0 (366.1); $[Cu(\mathbf{L^4SSL^4})]^+$ m/z 607.1 (607.2). UV−vis in CH_3CN at 1 mM [Cu] concentration: 254 nm (ε = 6900 M^{-1} cm^{-1}), 297 nm (ε = 2300 M^{-1} cm^{-1}).

■ ASSOCIATED CONTENT

Ⓢ Supporting Information

Crystallographic data of $[Cu^{II}_2(\mathbf{L^2S})_2](BF_4)_2 \cdot C_3H_6O$, $[Cu^{I}_2(\mathbf{L^4SSL^4})](BF_4)_2$, and $[Cu^{I}_2(\mathbf{L^3SSL^3})](BF_4)_2$ (CIF format); ligand synthesis scheme; VT NMR spectra with $\mathbf{L^2SSL^2}$; UV−vis spectra; and cyclic voltammograms. All Cartesian coordinates from DFT calculations including gas phase optimizations. This material is available free of charge via the Internet at http://pubs.acs.org.

■ AUTHOR INFORMATION

Corresponding Authors

*E-mail: c.fonsecaguerra@vu.nl.

*E-mail: bouwman@chem.leidenuniv.nl.

Notes

The authors declare no competing financial interest.

■ ACKNOWLEDGMENTS

This research has been financially supported by the National Research School Combination NRSC-Catalysis, a joint activity of the graduate research schools NIOK, HRSMC, and EPL. We thank Fanny Trausel for the synthesis of $[Cu^{I}_2(\mathbf{L^3SSL^3})](BF_4)_2$, John van Dijk for ESI-MS analysis, and Fons Lefeber and Karthick Sai Sankar Gupta for assistance with VT-NMR. We thank Prof. Dr. E. J. Baerends for helpful discussions. The

Netherlands Organization for Scientific Research (NWO-CW) is acknowledged for further financial support (NWO-BAZIS grant Amsterdam Laboratory for Computational Chemistry).

REFERENCES

(1) Solomon, E. I.; Sundaram, U. M.; Machonkin, T. E. *Chem. Rev.* **1996**, *96*, 2563−2606.
(2) Jacob, C.; Giles, G. L.; Giles, N. M.; Sies, H. *Angew. Chem., Int. Ed.* **2003**, *42*, 4742−4758.
(3) Bickelhaupt, F. M.; Sola, M.; Schleyer, P. V. *J. Comput. Chem.* **1995**, *16*, 465−477.
(4) Carvalho, A. T. P.; Swart, M.; van Stralen, J. N. P.; Fernandes, P. A.; Ramos, M. J.; Bickelhaupt, F. M. *J. Phys. Chem. B* **2008**, *112*, 2511−2523.
(5) Roos, G.; Fonseca Guerra, C.; Bickelhaupt, F. M. *J. Biomol. Struct. Dyn.* **2014**, in press. DOI: 10.1080/07391102.2013.851034.
(6) Iwata, S.; Ostermeier, C.; Ludwig, B.; Michel, H. *Nature* **1995**, *376*, 660−669.
(7) Katayama, Y.; Hashimoto, K.; Nakayama, H.; Mino, H.; Nojiri, M.; Ono, T.; Nyunoya, H.; Yohda, M.; Takio, K.; Odaka, M. *J. Am. Chem. Soc.* **2006**, *128*, 728−729.
(8) Shigehiro, S.; Nakasako, M.; Dohmae, N.; Tsujimura, M.; Tokoi, K.; Odaka, M.; Yohda, M.; Kamiya, N.; Endo, I. *Nat. Struct. Biol.* **1998**, *5*, 347−351.
(9) Brown, K.; Tegoni, M.; Prudencio, M.; Pereira, A. S.; Besson, S.; Moura, J. J.; Moura, I.; Cambillau, C. *Nat. Struct. Biol.* **2000**, *7*, 191−195.
(10) Blackburn, N. J.; de Vries, S.; Barr, M. E.; Houser, R. P.; Tolman, W. B.; Sanders, D.; Fee, J. A. *J. Am. Chem. Soc.* **1997**, *119*, 6135−6143.
(11) Ye, Q.; Imriskova-Sosova, I.; Hill, B. C.; Jia, Z. *Biochemistry* **2005**, *44*, 2934−2942.
(12) Cawthorn, T. R.; Poulsen, B. E.; Davidson, D. E.; Andrews, D.; Hill, B. C. *Biochemistry* **2009**, *48*, 4448−4454.
(13) Banci, L.; Bertini, I.; Cavallaro, G.; Ciofi-Baffoni, S. *FEBS J.* **2011**, *278*, 2244−2262.
(14) Jomova, K.; Valko, M. *Toxicology* **2011**, *283*, 65−87.
(15) Pedersen, J. T.; Hureau, C.; Hemmingsen, L.; Heegaard, N. H. H.; Østergaard, J.; Vašák, M.; Faller, P. *Biochemistry* **2012**, *51*, 1697−1706.
(16) Thomas, A. M.; Lin, B.-L.; Wasinger, E. C.; Stack, T. D. P. *J. Am. Chem. Soc.* **2013**, *135*, 18912−18919.
(17) Meloni, G.; Faller, P.; Vašák, M. *J. Biol. Chem.* **2007**, *282*, 16068−16078.
(18) Finkel, T.; Holbrook, N. J. *Nature* **2000**, *408*, 239−247.
(19) Ording-Wenker, E. C. M.; Siegler, M. A.; Lutz, M.; Bouwman, E. *Inorg. Chem.* **2013**, *52*, 13113−13122.
(20) Gennari, M.; Pecaut, J.; DeBeer, S.; Neese, F.; Collomb, M.-N.; Duboc, C. *Angew. Chem., Int. Ed.* **2011**, *50*, 5661−5665.
(21) Houser, R. P.; Halfen, J. A.; Young, V. G.; Blackburn, N. J.; Tolman, W. B. *J. Am. Chem. Soc.* **1995**, *117*, 10745−10746.
(22) Rammal, W.; Belle, C.; Beguin, C.; Duboc, C.; Philouze, C.; Pierre, J.-L.; Le Pape, L.; Bertaina, S.; Saint-Aman, E.; Torelli, S. *Inorg. Chem.* **2006**, *45*, 10355−10362.
(23) Ohta, T.; Tachiyama, T.; Yoshizawa, K.; Yamabe, T. *Tetrahedron Lett.* **2000**, *41*, 2581−2585.
(24) Neuba, A.; Haase, R.; Meyer-Klaucke, W.; Flörke, U.; Henkel, G. *Angew. Chem., Int. Ed.* **2012**, *51*, 1714−1718.
(25) Ueno, Y.; Tachi, Y.; Itoh, S. *J. Am. Chem. Soc.* **2002**, *124*, 12428−12429.
(26) Osako, T.; Ueno, Y.; Tachi, Y.; Itoh, S. *Inorg. Chem.* **2004**, *43*, 6516−6518.
(27) Itoh, S.; Nagagawa, M.; Fukuzumi, S. *J. Am. Chem. Soc.* **2001**, *123*, 4087−4088.
(28) Willcocks, A. M.; Johnson, A. L.; Raithby, P. R.; Schiffers, S.; Warren, J. E. *Acta Crystallogr., Sect. C* **2011**, *67*, 215−217.
(29) Colak, A. T.; Yesilel, O. Z.; Buyukgungor, O. *J. Mol. Struct.* **2011**, *991*, 68−72.
(30) Chou, C.-C.; Liu, H.-J.; Su, C.-C. *Dalton Trans.* **2008**, 3358−3362.
(31) Creaven, B. S.; Mahon, M. F.; McGinley, J.; Moore, A. M. *Inorg. Chem. Commun.* **2006**, *9*, 231−234.
(32) Evans, D. F. *J. Chem. Soc.* **1959**, 2003−2005.
(33) Bain, G. A.; Berry, J. F. *J. Chem. Educ.* **2008**, *85*, 532−536.
(34) Lee, D. H.; Wei, N.; Murthy, N. N.; Tyeklar, Z.; Karlin, K. D.; Kaderli, S.; Jung, B.; Zuberbuhler, A. D. *J. Am. Chem. Soc.* **1995**, *117*, 12498−12513.
(35) Sheldrick, G. M. *Acta Crystallogr., Sect. A* **2008**, *64*, 112−122.
(36) te Velde, G.; Bickelhaupt, F. M.; Baerends, E. J.; Guerra, C. F.; Van Gisbergen, S. J. A.; Snijders, J. G.; Ziegler, T. *J. Comput. Chem.* **2001**, *22*, 931−967.
(37) http://www.scm.com/.
(38) Swart, M.; Ehlers, A. W.; Lammertsma, K. *Mol. Phys.* **2004**, *102*, 2467−2474.
(39) Klamt, A. *J. Phys. Chem.* **1995**, *99*, 2224−2235.
(40) Klamt, A.; Schuurmann, G. *J. Chem. Soc., Perkin Trans. 2* **1993**, 799−805.
(41) Pye, C. C.; Ziegler, T. *Theor. Chem. Acc.* **1999**, *101*, 396−408.
(42) Swart, M.; Roesler, E.; Bickelhaupt, F. M. *Eur. J. Inorg. Chem.* **2007**, 3646−3654.
(43) Noodleman, L. *J. Chem. Phys.* **1981**, *74*, 5737−5743.
(44) Noodleman, L.; Baerends, E. J. *J. Am. Chem. Soc.* **1984**, *106*, 2316−2327.
(45) Jensen, F. *Introduction to Computational Chemistry*, 2nd ed.; Wiley: Chichester, West Sussex, U.K., 2006.